J. Fluid Mech. (1993), *vol.* 250, *pp.* 481–508

Vortex-induced vibrations of a long flexible circular cylinder

By D. BRIKA AND A. LANEVILLE

Département de génie mécanique, Université de Sherbrooke, Sherbrooke, Québec, J1K 2R1, Canada

(Received 10 May 1991 and in revised form 20 November 1992)

In an experimental study of the vortex-induced oscillations of a long flexible circular cylinder, the observed stationary amplitudes describe an hysteresis loop partially different from earlier studies. Each branch of the loop is associated with a vortex shedding mode and, as a jump from one branch to the other occurs, the phase difference between the cylinder displacement and the vortex shedding undergoes an abrupt change. The critical flow velocities at which the jump occurs concur with the flow visualization observations of Williamson & Roshko (1988) on the vortex shedding modes near the fundamental synchronization region. Impulsive regimes, obtained at a given flow velocity with the cylinder initially at rest or pre-excited, and progressive regimes resulting from a variation of the flow velocity, are examined. The occurrence of bifurcations is detected for a flow velocity range in the case of the impulsive regimes. The coordinates of the bifurcations define a boundary between two vortex shedding modes, a boundary that verifies the critical curve obtained by Williamson & Roshko (1988). The experimental set-up of this study simulates half the wavelength of a vibrating cable, eliminates the end effects present in oscillating rigid cylinder set-up and has one of the lowest damping ratios reported for the study of this phenomenon.

1. Introduction

Since long flexible cables are commonly used in engineering applications, especially in suspension bridges and electrical power transmission lines, there are numerous studies of their interaction with a fluid flow and the resulting oscillatory instabilities (see the reviews by Parkinson 1989; Bearman 1984; Sarpkaya 1979; and Blevins 1977, p. 363, among others). When exposed to wind, cables of circular cross-section, as any aerodynamically bluff body, are characterized by a flow separation from their surface and a wake carrying shed vortices downstream. The formation of these vortices results from the rollup of the unstable shear layers generated at the flow separation and this phenomenon induces an alternating pressure loading on the cylinder surface and a transverse force at frequency f_{vs}. For a long stationary circular cylinder, the vortex shedding frequency, f_{vs}, matches the frequency f_s defined by S, the Strouhal number ($S = f_s D/V$ where V is the oncoming wind velocity and D the geometrical characteristic of the cylinder). As the vortex shedding frequency approaches the natural frequency of a given flexible circular cylinder, a resonant response tends to develop freely and, for a narrow range of air velocities, can reach amplitudes of the order of $1D$ while the vortex shedding frequency locks-in to the cylinder frequency. This synchronization is part of a nonlinear phenomenon featuring an hysteresis loop.

The experiments on free vortex-induced vibrations conducted by Feng (1968) are well known, as are those on forced vibrations by Bishop & Hassan (1964*b*). In these

two sets of experiments, the observed hysteresis loop is characterized by simultaneous jumps in the cylinder vibration amplitude (A), in the lift and drag forces, as well as in the phase between the excitation and the cylinder displacement. The position of the jumps is influenced by whether the velocity U is increased from lower velocities or decreased from higher velocities ($U = V/2\pi fD$ where f is the cylinder vibration frequency). This hysteresis loop can admittedly be attributed to nonlinear spring or damping behaviour: forced nonlinear vibrations governed by Duffing's equation (Holmes & Rand 1976) can exhibit such an hysteresis loop. However, in an analysis of Feng's results, Parkinson (1989) suggests that the hysteresis conditioning originates from the fluid system, therefore from the lift forces, not from the model elastic system. By modelling the fluid system by a nonlinear wake oscillator in combination with the equation of motion of a mass–spring–damper system, Hartlen & Currie (1970), Landl (1975) and Berger (1984) among others, have had some success in producing results qualitatively similar to those obtained experimentally. In spite of this relative success, the arguments invoked in establishing the wake oscillator are not altogether convincing (Sarpkaya 1979 and Parkinson 1989).

From the analysis of flow visualization films of Den Hartog (1934), Meier-Windhorst (1939), Angrilli, Di Silvio & Zanardo (1974) and Griffin & Ramberg (1974), Zdravkovich (1982) observes the occurrence of a drastic change in the structure of the shed vortices as a phase jump takes place. Öngören & Rockwell (1988*a*) observed more in detail this change in the vortical structure of the near wake on either side of the phase jump.

Williamson & Roshko (1988), in the interpretation of their flow visualization results, also provide an explanation for the hysteresis loop in terms of a change in the configuration of the vortex wake. The phase jump is attributed to a sudden change in the wake patterns, specifically in the modes denoted as 2S and 2P. The 2S mode is associated with flow regimes in which, for each half-cycle, a vortex is fed into the downstream wake, like Kármán vortex shedding, while the 2P mode is associated with flow regimes in which vortex pairs are formed in the near wake and 'convect laterally outwards from the wake centerline'. These experimental results suggest that the hysteresis has its source in a fluid mechanic phenomenon.

Simulations of the eolian vibrations of cables were performed mostly with a rigid cylinder. Very few attempts have been made to simulate half the wavelength of the vibrating cable in a wind tunnel. Rawlins (1983) reports such wind tunnel tests and measurements of the aerodynamic damping. Since the end effects associated with the oscillations of an elastically mounted rigid cylinder close to a wall can be a source of flow non-uniformities, a more appropriate approach might be to use a flexible cylinder with the nodes of its first free–free vibration mode located at the tunnel walls in order to simulate the eolian oscillations of long cables. Half of the stationary waves present in the cable motion are then well reproduced. The work reported here deals with such an experimental simulation and examines the hysteresis under a different set of conditions. The results are compared to those of Feng (1968) and Bishop & Hassan (1964*a*, *b*) and then discussed in the light of the different vortex shedding patterns observed by Williamson & Roshko (1988). The present results confirm that the hysteresis loop is a fluid-mechanic phenomenon.

2. Experimental set-up and methodology

The experimental set-up shown in figure 1 is similar to the one used by Rawlins (1983). It consists of a long circular tube with characteristics: external diameter, $D =$

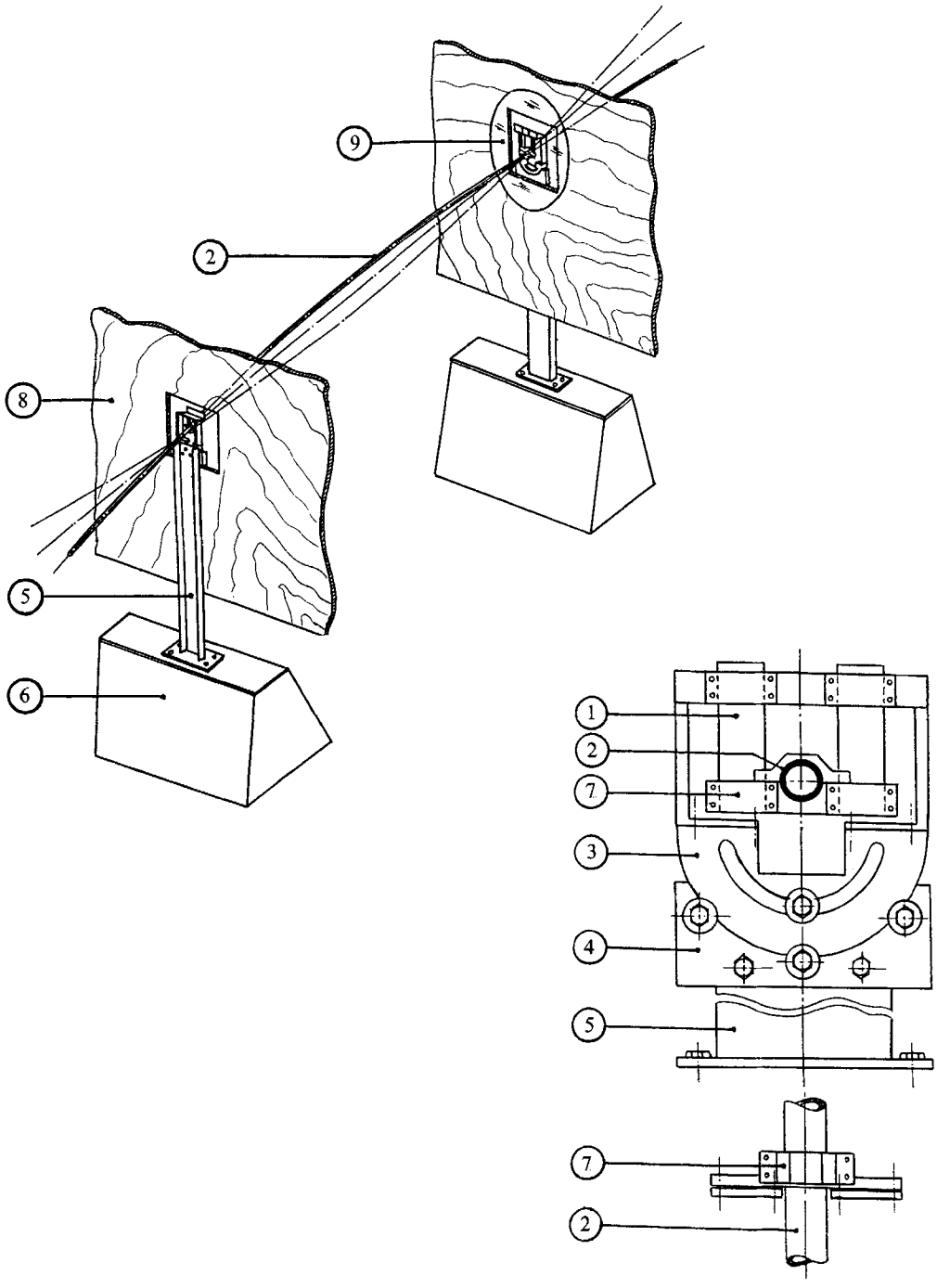

FIGURE 1. Schematic view of the experimental set-up: 1, steel flexible blade; 2, model; 3, 4, system adjustment blocks; 5, supporting beam; 6, concrete block; 7, clamp attachment; 8, wind tunnel wall; 9, streamlined shroud.

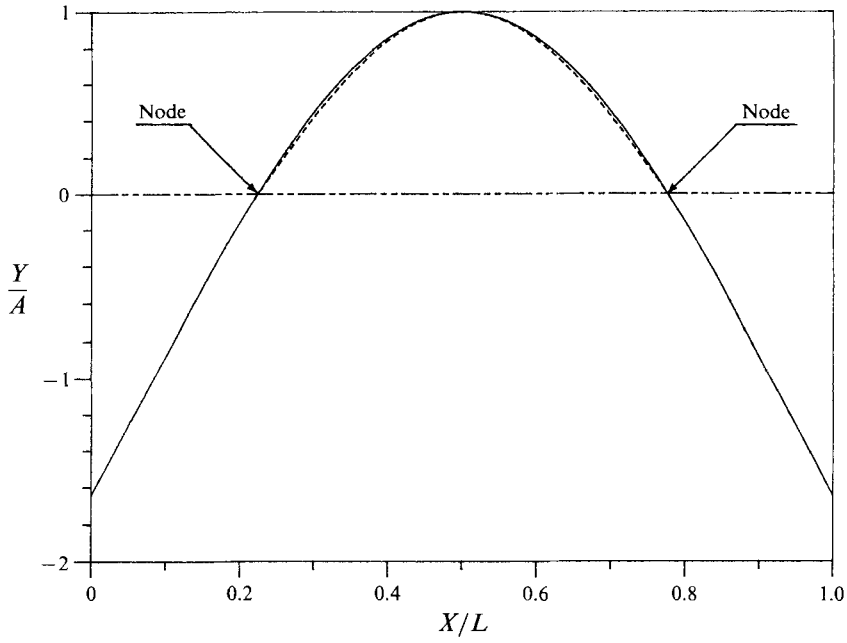

FIGURE 2. Mode shape of test model compared to the sinusoidal mode: ——, first free–free mode shape; – – – –, sine mode shape.

33.4 mm; internal diameter, $d = 26.6$ mm; total length, $L = 3.313$ m; mass per unit length, $m_L = 0.864$ kg/m; density $\rho_s = 4\,m_L/\pi(D^2 - d^2) = 2697$ kg/m^3.

The tube is suspended by thin steel flexible blades at the nodal points of its first free–free vibration mode and spans horizontally the complete wind tunnel square test section (1.83 × 1.83 m) in its centre. The total length, L, is chosen to fix the nodal points at the wall. The resultant natural frequency for this mode is

$$f_n = 17.58 \text{ Hz}.$$

In order to isolate the vertical suspension blades from the wind tunnel airflow, a cover with a 40 mm hole allowing for the cylinder's way is mounted on the tunnel wall. The net length of the cylinder exposed to the airflow, L_v, is then 1.76 m giving an aspect ratio $L_v/D = 52.7$.

The suspension system made of wide spring steel blades allows a transversal motion of the cylinder but prevents its motion in the streamwise flow direction.

This experimental approach allows the exposed cylinder portion to oscillate with a quasi-sinusoidal form and is a closer simulation of cable vibrations. The equation for this first mode is

$$\frac{Y}{A} = 0.8226\left[\left(\cosh\frac{KX}{L} + \cos\frac{KX}{L}\right) - \sigma\left(\sinh\frac{KX}{L} + \sin\frac{KX}{L}\right)\right] \tag{1}$$

with $K = 4.73$, $\sigma = 0.9825$, X the longitudinal distance from one end of the model, and A the single amplitude at midspan.

The form is compared to the sinusoidal form in figure 2 and the largest difference in Y/A is 2.9%.

The cylinder oscillations are measured with a B&K 4393 accelerometer (mass = 2.4 g) located on the cylinder at 45 mm from the nodal point outside the wind tunnel.

The accelerometer output is fed to a B&K 2635 charge amplifier to obtain the vibration amplitude. The spectral analysis of the response is performed on a B&K 2032 frequency analyser.

For tests at a given air velocity, the cylinder vibrations are obtained either from rest or from an artificial excitation. The shaker (B&K 4809), which can be quickly uncoupled from the model, is driven by a power amplifier (B&K 2706) coupled to a wave generator delivering a sinusoidal signal matching the cylinder natural frequency. The mechanical excitation is applied at a point on the cylinder located 130 mm from the nodal point outside the tunnel wall.

To establish the vortex regime in the near wake of the oscillating cylinder, smoke is used to visualize the flow. Video recordings are taken as the cylinder near wake is 'frozen' by a stroboscope (strobolume GR 1540) triggered by the accelerometer signal. The strobolume is equipped with an oscillator/delay unit allowing the adjustment of the cylinder position.

The vortex shedding frequency is obtained with a hot-wire anemometer (one component normal to the flow) located at the model midspan, $1D$ downstream and $1D$ below the stationary cylinder axis. The phase difference between the hot-wire output and the accelerometer signal is also recorded. The measured phase difference remains a relative characteristic since the anemometer is stationary and at a distance from the cylinder in motion. The measured phase difference is then influenced by the cylinder position and the air velocity via a time delay. This can be avoided only if the transducer is flush mounted on the cylinder surface and compensated for inertial effects. The model used in this study does not allow for such a set-up. For a fixed hot wire, this time delay varies inversely with the air velocity, or the velocity at which the vortices are transported in the wake. The phase results may be corrected according to

$$\Delta\Phi = \Delta\Phi_{\mathrm{R}} + \frac{\partial\Phi}{\partial U}(U - U_{\mathrm{R}}) + \frac{\partial\Phi}{\partial(A/D)}[(A/D) - (A/D)_{\mathrm{R}}], \tag{2}$$

where, for the present set-up, $\Delta\Phi_{\mathrm{R}} = 34°$, $U_{\mathrm{R}} = 0.78$, $(A/D)_{\mathrm{R}} = 0$,

$$\frac{\partial\Phi}{\partial U} = -\frac{57}{U^2}\,(\mathrm{deg}), \quad \frac{\partial\Phi}{\partial(A/D)} = 22\,(\mathrm{deg}).$$

The first term on the right-hand side includes all the time lags associated with the electronics and the tubing length as well as the reference phase lag when the cylinder is practically at rest and not experiencing the beating phenomenon. This term is evaluated for $U = 0.78$, the synchronization onset velocity, and $\Delta\Phi$ is assumed zero under these conditions. The second term takes care of the effect of air velocity change and the third takes into account the vertical displacement of the cylinder. The correction formula is empirical and its derivatives were determined from experimental data (Brika 1990).

The upstream air velocity is measured, and so is the cylinder base pressure with standard pressure transducers. The test conditions were: upstream air velocity, $1.6 \leqslant V \leqslant 5.5$ m/s; Reynolds number, $3400 \leqslant Re \leqslant 11\,800$.

The system damping is obtained by measuring the logarithmic decrement δ_0 as the cylinder is vibrating in still air. The damping measured in these conditions includes the structural damping and the aerodynamic damping associated with the drag of the oscillating cylinder. It can be divided in a portion, δ_{B}, a base value which is independent of the vibration amplitude and δ_A, a portion proportional to the square of the vibration amplitude:

$$\delta_0 = \delta_{\mathrm{B}} + \delta_A. \tag{3}$$

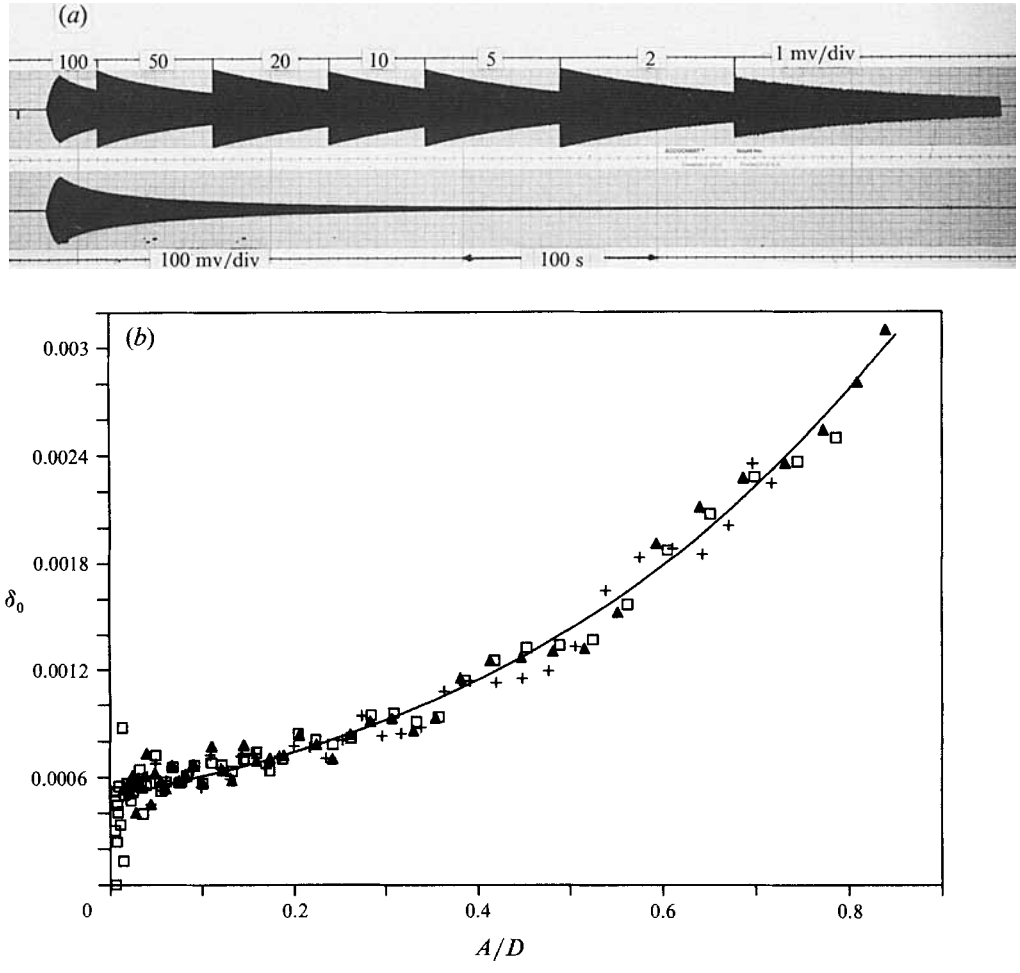

FIGURE 3. The system damping in still air. (*a*) Record of the cylinder displacement in still air; (*b*) total logarithmic decrement *vs.* dimensionless midspan amplitude A/D. □, test A; +, test B; ▲, test C; ——, fitting curve.

The damping portion, δ_B, can be estimated from the recordings of the cylinder vibrating at small amplitude. It is made up of the structural damping, δ_S, and the 'aerodynamic' viscous damping:

$$\delta_B = \delta_S + \frac{4\pi\sqrt{2}}{(Re_\omega)^{\frac{1}{2}}}\frac{\rho}{\rho_s}\frac{1}{1-(d/D)^2}, \tag{4}$$

where $Re_\omega = 2\pi\beta = \omega_n D^2/\nu = 8326$, $\omega_n = 2\pi f_n$, β is the Stokes number, ν the fluid kinematic viscosity, and ρ the fluid density.

The second term on the right-hand side comes from Batchelor (1968, p. 357), and has a value of 2.32×10^{-4} which accounts for 45% of δ_B ($\delta_B = 5.2\times10^{-4}$ by an extrapolation of the curve of figure 3). This basic logarithmic decrement, δ_B, is of the same order as that for a similar system (6.6×10^{-4}) used by Rawlins (1983).

Since the lengths of the cylinder outside the wind tunnel during the tests are in still air, the damping due to these lengths becomes part of the system damping. For an

oscillating cylinder, the portion of aerodynamic damping which is a quadratic function of the amplitude (Sarpkaya 1979), can be expressed per unit length as:

$$\delta_A = 2.12\frac{\rho}{\rho_s}(A/D)^2 \tag{5}$$

and after an integration over L, the cylinder length, one gets for P_D, the power dissipated by this portion of the aerodynamic damping, taking into account the node location X_n:

$$\begin{aligned} P_D &= 2LA^4K_c\left(\int_0^{X_n/L}\left(\frac{Y}{A}\right)^4 \mathrm{d}\left(\frac{X}{L}\right)+\int_{X_n/L}^{\frac{1}{2}}\left(\frac{Y}{A}\right)^4 \mathrm{d}\left(\frac{X}{L}\right)\right) \\ &= 2LA^4K_c(0.3164+0.1078), \end{aligned} \tag{6}$$

where

$$K_c = \frac{2.5}{3\pi}\rho\omega_n^3.$$

The damping due to the cylinder lengths external to the wind tunnel and vibrating in this given mode accounts for 75% of δ_A in free air; this agrees with the amount obtained by Rawlins (1983). The system damping with the model exposed partly to the wind tunnel flow is then

$$\delta_{\text{system}} = \delta_B + 0.75\delta_A. \tag{7}$$

In the range $0 < A/D < 0.52$, the aerodynamic logarithmic decrement, as shown in figure 3, varies between 0 and 9.75×10^{-4} and the damping ratio ζ of the system, between 0.83×10^{-4} and 2×10^{-4}. This damping is one order of magnitude smaller than that of the system used by Feng (1968). In terms of the Scruton number, Sc, defined as $2\pi\zeta/n$ with $n = \rho D^2/2m_L^* = 0.00031$, it represents a variation from 1.69 at small amplitudes ($A/D \sim 0$) to 4.06 for the maximum displacement ($A/D \sim 0.52$). For this last amplitude, the Scruton number in the present tests is 15% higher than that for Feng's system with light damping ($Sc = 3.52$). The Scruton number is a measure of the ability of lightweight structures to damp flow-induced vibrations. Large Scruton numbers are generally associated with small-amplitude flow-induced vibrations. In the present calculation of the Scruton number, an equivalent mass per unit length, m_L^*, is adopted to take into account that the energy extracted by the portion of the cylinder vibrating in a sinusoidal mode shape within the wind tunnel is distributed over its whole length. The equivalent mass per unit length is then defined as:

$$m_L^* = m_L\int_0^{L/2} Y^2\,\mathrm{d}X \Big/ \int_{X_n}^{L/2} Y^2\,\mathrm{d}X = 2.37m_L, \tag{8}$$

where Y is given by equation (1), the first free–free vibration mode shape.

The tests are performed using one of the following four procedures: (i) fixed air velocity and cylinder released from rest; (ii) fixed air velocity and cylinder artificially excited and released; (iii) with the cylinder in its steady-state amplitude, small increment of the air velocity; (iv) same as (iii) but small decrement of the air velocity. Procedures (i) and (ii) are referred to as 'impulsive regimes' and procedures (iii) and (iv) as 'progressive regimes'.

Most of the results presented will be for steady-state amplitudes of oscillations. The blockage ratio of the model to the test section is small, of the order of 1.8% but the air velocity is corrected according to the method proposed by Pankhurst & Holder (1962).

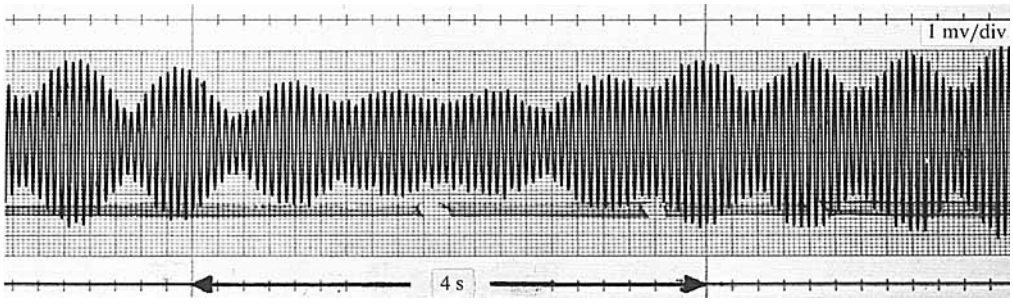

FIGURE 4. The beating phenomenon observed at the synchronization onset ($U = 0.74$).

3. Results

The experimental results will be presented according to the test procedures, i.e. impulsive regimes and progressive regimes.

For air velocities U lower than 0.78 or larger than 1.2, where U is the non-dimensional variable $U = V/2\pi fD$, the cylinder remains stationary and the vortex shedding frequency is represented by f_s, the Strouhal frequency. The frequency f is the cylinder oscillating frequency, nearly f_n in the present set-up.

3.1. *Progressive regimes*

For air velocities near $U = 0.78$, the synchronization onset velocity, the cylinder vibration amplitude shows a modulation, typically a beating which indicates the proximity of f_s to f_n (see figure 4).

Figure 5 shows traces of the vibration amplitude, the phase difference between the vortex shedding and the cylinder oscillations, and the base pressure, as the air velocity is progressively varied (procedures iii and iv). In this figure, the recorder is stopped each time the air velocity is incremented (parts *a* and *b* of the figure) or decremented (part *c*).

Parts (*a*) and (*b*) indicate an increasing vibration amplitude with increasing air velocity, a tendency followed until the event of a change in phase between the vortex shedding and the cylinder displacement. Past this event, an increase of the air velocity produces a small reduction in the cylinder amplitude. The record of the phase angle shows some fluctuations in the earlier stages of synchronization and as the flow velocity is increased, the phase angle varies slightly, up to three peaks, announcing an approaching change of phase at $U \approx 1$ (or competition between modes of vortex shedding). Past the change of phase, the phase angle does not show as a fluctuating component as for $U < 1$. The trace of the base pressure signal shows a progressive variation, initially with small fluctuations and then with increasing fluctuations as the change in phase is approached. Past the change in phase, the base pressure signal, like the phase angle, fluctuates much less. These results, as expected, indicate that the wake organization plays a major role in this phenomenon.

Figure 5(*c*) shows the case of procedure (iv) in which the velocity is decreased progressively. As the initial condition, $U > 1.0$, is modified, a reduction of U produces a small increase in the cylinder vibration amplitude, down to a change in phase where the amplitude is reduced by almost 60%. With further reductions of the air velocity, the cylinder amplitude reduces. Prior to the phase change, the phase angle signal remains very regular while, for lower velocities, this signal is very fluctuating. The base pressure signal shows almost no fluctuations as the air velocity is decreased and this

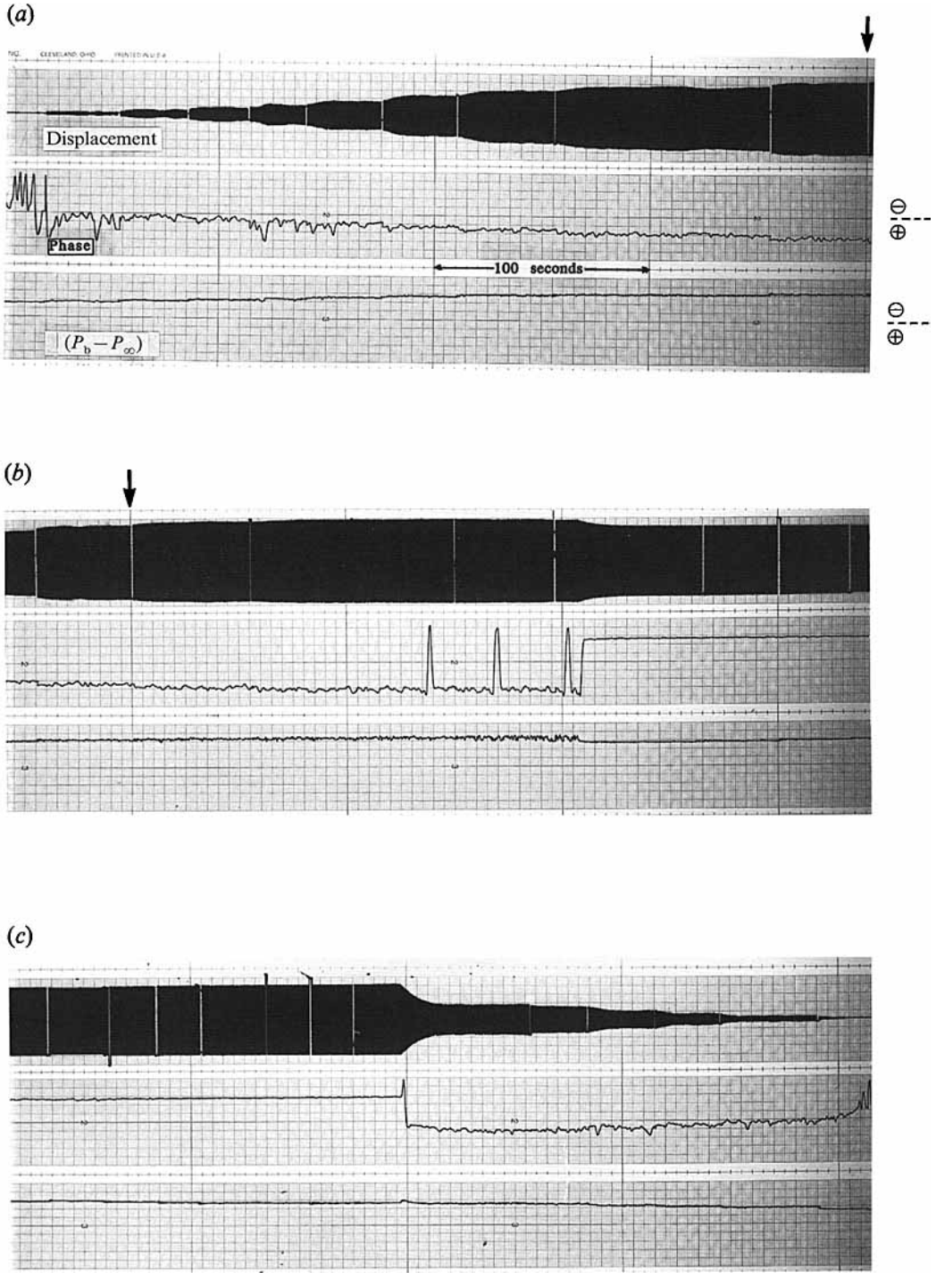

FIGURE 5. Traces of the vibration amplitude A, the phase angle Φ and the pressure difference $(P_b - P_\infty)$ for progressive regimes: (*a*) and (*b*), increasing velocity; (*c*), decreasing velocity.

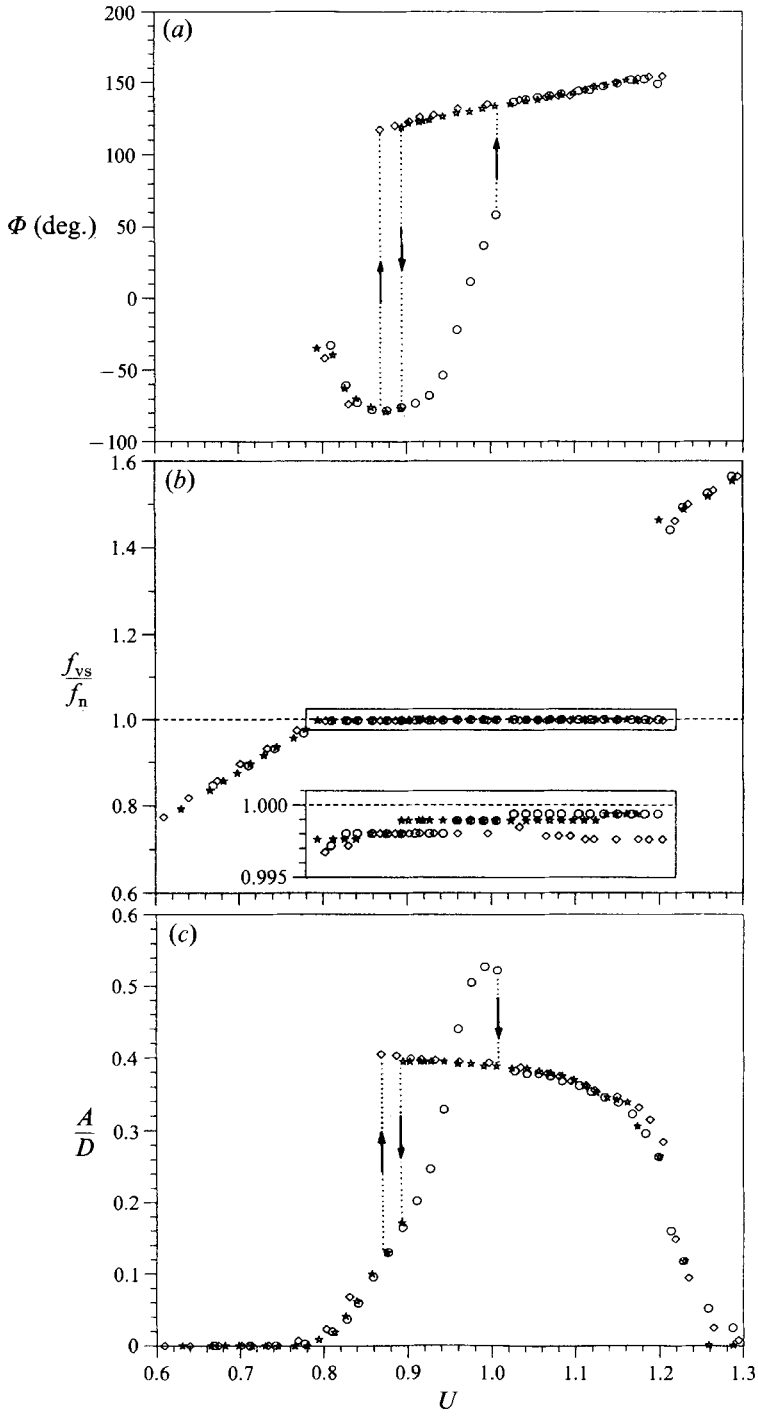

FIGURE 6. (*a*) The phase angle Φ, (*b*) the ratio of the vortex shedding frequency to the system natural frequency f_{vs}/f_n and (*c*) the relative vibration amplitude A/D versus the relative velocity U: ○, increasing velocity; ☆, decreasing velocity; ◇, increasing velocity with large steps.

behaviour differs from the results obtained with procedure (iii) shown in parts (*a*) and (*b*).

The steady-state results for the progressive regimes, i.e. the phase angle Φ, the ratio of the vortex shedding frequency to the cylinder natural frequency and the relative amplitude of vibration are presented in figure 6 as functions of the velocity U, and will be discussed according to the incremental value of U. The time-mean base pressure coefficient will also be presented.

3.1.1. *Small increments of U*

For small increments of U, $\Delta U \approx 0.02$ (shown as circles), the cylinder begins to oscillate at $U \approx 0.78$ and as the air velocity is incremented towards $U \approx 1$, its amplitude grows rapidly following the upper branch of an hysteresis loop. For $U \approx 1$, the upper critical velocity (UCV), the reduced amplitude is 0.53 and drops abruptly to 0.38 onto the lower branch of the hysteresis loop. A further increase of the air velocity brings about a reduction of the amplitude. From $U = 1.02$ to 1.20, this reduction is not as severe as in the range $1.20 < U < 1.30$, for which the steady-state conditions are obtained after a long time. Past $U = 1.30$, the vortex-induced vibrations disappear.

Figure 6(*b*) shows the phenomenon of synchronization in the range $0.78 < U < 1.2$ as the cylinder frequency modulates the vortex shedding frequency. In this range of velocity, the vortex shedding frequency, although very close to the cylinder natural frequency, varies slightly (0.15%) as indicated by the inset. Outside the lock-in region, the vortex shedding frequency matches the Strouhal frequency. The earlier drop in amplitude observed at $U \approx 1$ is accompanied by a jump of 75° in the phase angle. Again these results indicate that the wake organization plays a dominant role in vortex-induced vibrations.

3.1.2. *Small decrements of U*

For decreasing velocities from $U > 1.3$ (star symbols), it can be observed that the steady vibration amplitudes are similar to those for increasing U in the range $U \geqslant 1$. In the neighbourhood of the UCV, the amplitude ceases to follow the curve defined by the increasing velocity tests; it does not jump from 0.38 to 0.53, and the phase change does not occur. The air velocity has to be reduced to $U = 0.89$, the lower critical velocity (LCV), for this phase change to occur, accompanied by a 57% reduction of the amplitude (A/D decreasing from 0.39 to 0.17). Additional tests (Brika 1990) have shown the LCV to be in the range $0.87 < U < 0.89$. Lock-in is present for the whole range $0.78 < U < 1.2$. The plateau defined by the amplitude of vibration $A/D = 0.39$ ($\pm 1.7\%$ in the region $0.89 < U < 1.0$) intercepts the curve obtained with small increments of U at the coordinates $A/D = 0.39$ and $U = 0.96$.

3.1.3. *Large increments of U*

If ΔU, the increment of the velocity, is increased by a factor of two near the onset of synchronization, the resulting data for the progressive regime (lozenge symbols in figure 6) no longer correspond to the observations in §3.1.1. As the air velocity U is increased, the data follow the common branch of the loop up to $U = 0.87$ and then jump to the lower branch of the loop, without accessing the upper branch for any larger value of U. This jump is also accompanied by a phase change. This behaviour, observed in few cases, indicates that close to the lower critical velocity, the flow regime associated with the upper branch becomes susceptible to velocity perturbations ($\Delta U \sim 0.03$) and surrenders to the flow regime associated with the lower branch.

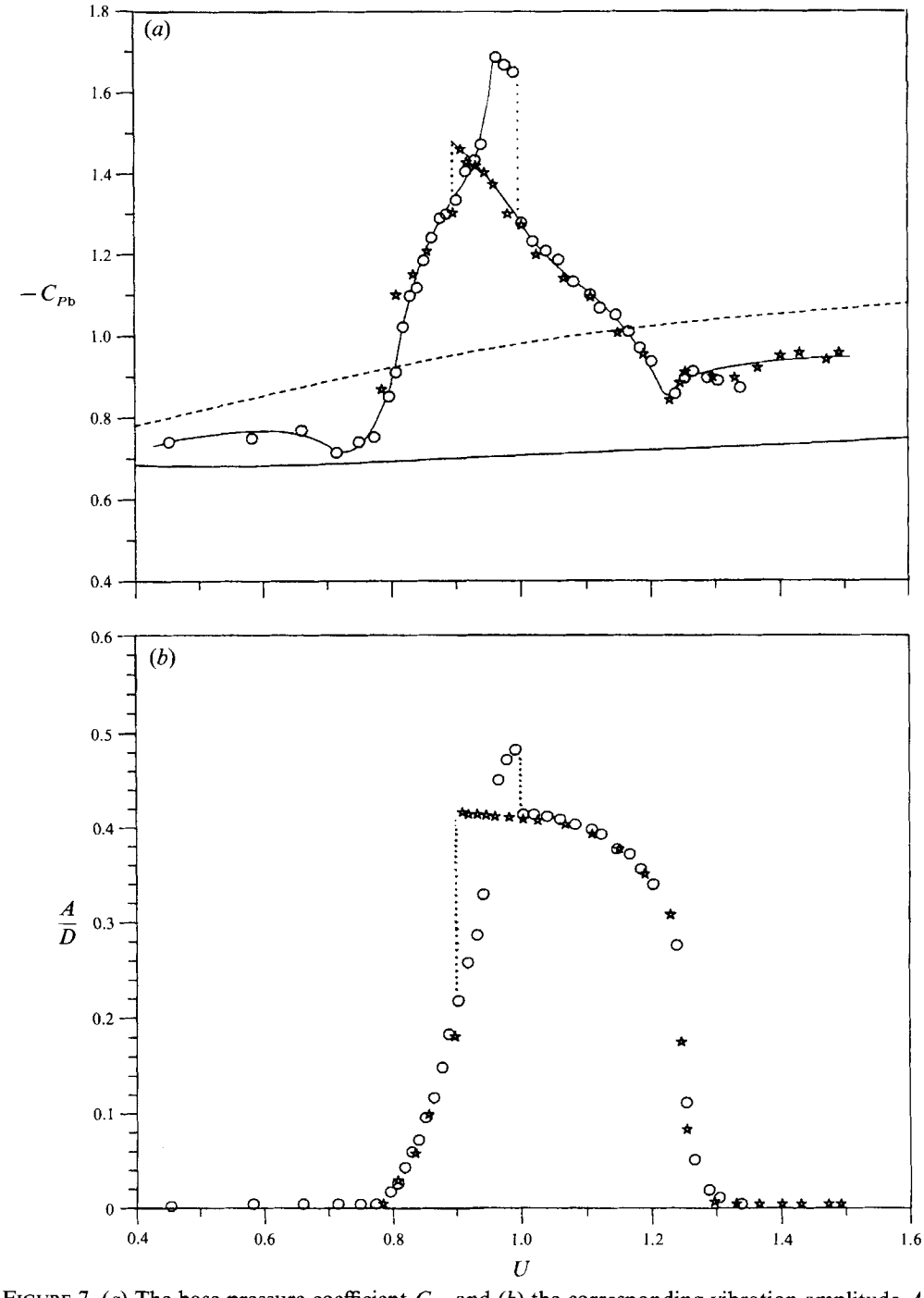

FIGURE 7. (*a*) The base pressure coefficient C_{Pb} and (*b*) the corresponding vibration amplitude A/D as functions of the velocity U: ○, increasing velocity; ☆, decreasing velocity; ——, stationary cylinder with very low free-stream turbulence and polished cylinder surface (Chen 1972); – – – –, stationary cylinder with high free-stream turbulence and very rough cylinder surface (Chen 1972).

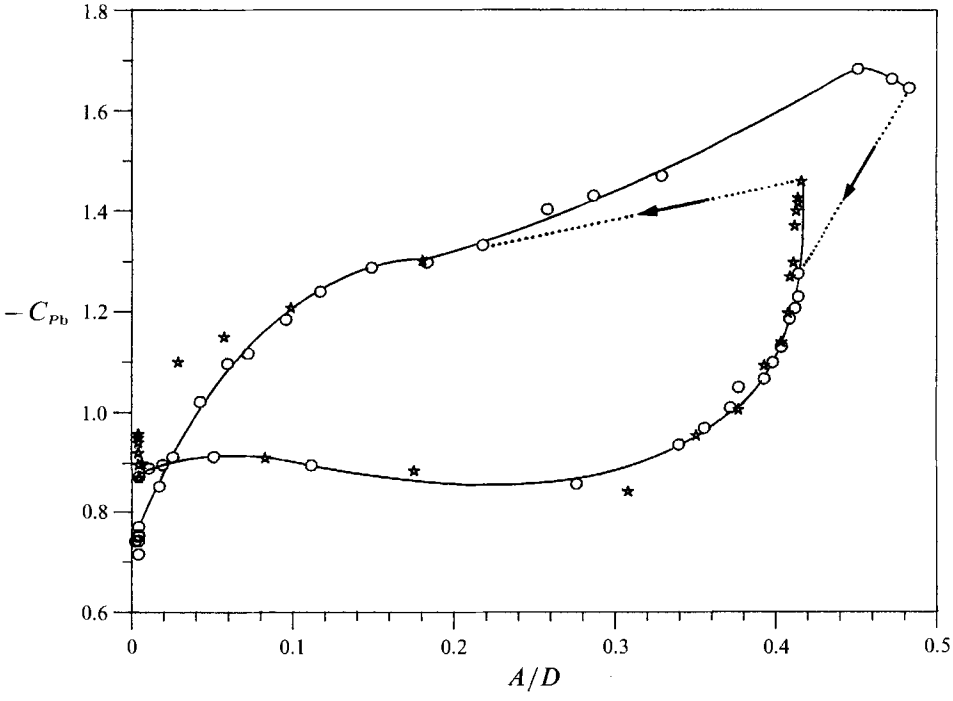

FIGURE 8. The relationship between the base pressure coefficient C_{Pb} and the dimensionless amplitude A/D (symbols as in figure 7).

3.1.4. *Base pressure coefficient* C_{Pb}

Figure 7 shows the data from a limited series of tests in which the base pressure is measured by a small 2 mm diameter tube fixed to the most downstream point of the cylinder at its midspan. The protuberance resulting from this tube did not affect significantly the vibration amplitudes when compared to the amplitudes obtained with the bare cylinder. The base pressure coefficient, C_{Pb}, is given by

$$C_{Pb} = \frac{P_b - P_\infty}{\frac{1}{2}\rho V^2}, \tag{9}$$

where P_b and P_∞ are respectively the base pressure and the static pressure of the oncoming flow. As for the stationary oscillations, an hysteresis is present in the $C_{Pb}(U)$ curve with its discontinuities concurring with the jumps in the amplitude curve.

The base pressure coefficient is significantly larger than in the case of the stationary cylinder as observed by Stansby (1976). Figure 8 shows the C_{Pb} (A/D) curve and supports the argument that the hysteresis observed during synchronization has its roots in the flow regime.

3.2. *Impulsive regimes*

These regimes are obtained when, for a fixed air velocity U, the flexible cylinder is either released from rest or externally excited by a shaker at an amplitude A/D of the order of 0.85 and then released. The results for the steady-state amplitudes are compared to the results for the progressive regimes in figure 9.

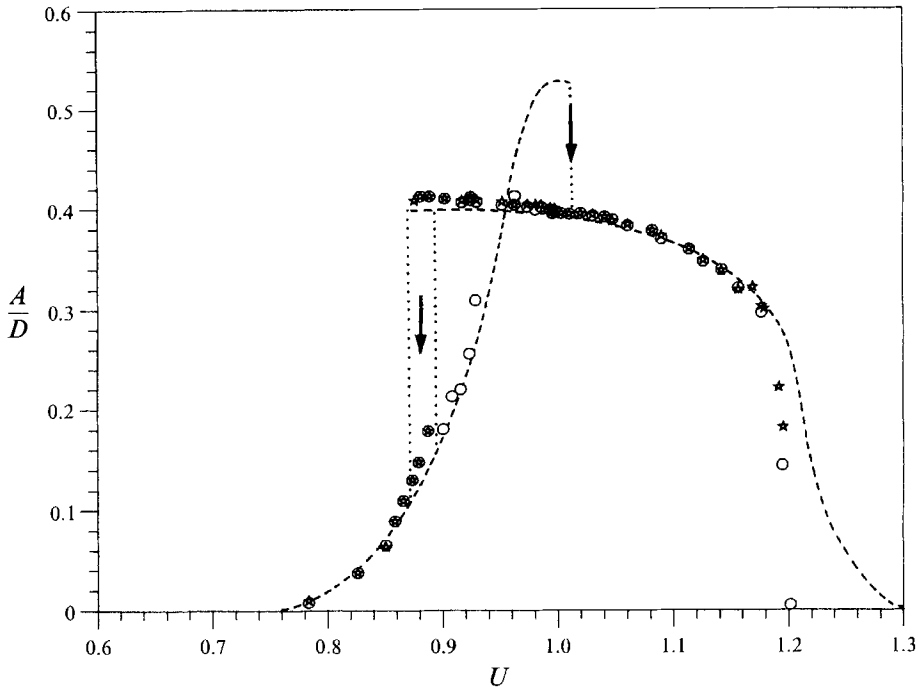

FIGURE 9. The steady-state vibration amplitude A/D of the impulsive regimes as a function of the velocity U compared to the results of the progressive regime: ☆, from rest; ○, from a pre-excited amplitude; ———, progressive regime.

3.2.1. *Free oscillations from rest (procedure i)*

For a cylinder released from rest and exposed to a given U, the steady-state vibration amplitude (figure 9, star symbols) is unique and its value is defined by the lower branch of the hysteresis loop if U is larger than or equal to the LCV ($U = 0.88$) or by the upper branch if U is smaller than the LCV. Figure 11 (*a*) shows a typical record for $U = 0.915$.

For velocities larger than the synchronization onset velocity ($U = 0.78$) and smaller than the LCV, the recordings of the amplitude build-up from rest show intriguing behaviour (figure 10): while the system tends towards a first but unavailable final state on an imaginary extension of the lower branch ($U <$ LCV), it suddenly departs, at a point defined by a break in the envelope curve, towards a second and available steady state of the upper branch. These bifurcations, or breaks in the envelope curves are accompanied by an abrupt change in the phase angle and indicate again a change in the wake flow regime.

3.2.2. *Free oscillations with pre-excitation (procedure ii)*

The steady-state amplitudes of these tests are shown by the circle symbols in figure 9. If U is smaller than the LCV, the cylinder stationary amplitude follows the upper branch of the hysteresis loop. When $U > 0.96$, the stationary oscillation amplitudes are described by the lower branch of the hysteresis loop.

In the narrow range of velocity 0.88 (LCV) $\leqslant U \leqslant 0.95$, there are two possible steady-state amplitudes for a given air velocity with this procedure.

Figure 11 shows some typical traces of the amplitudes as functions of time at $U =$ 0.92. Figure 11 (*a*) shows the case of the cylinder starting from rest and figure 11 (*b–d*),

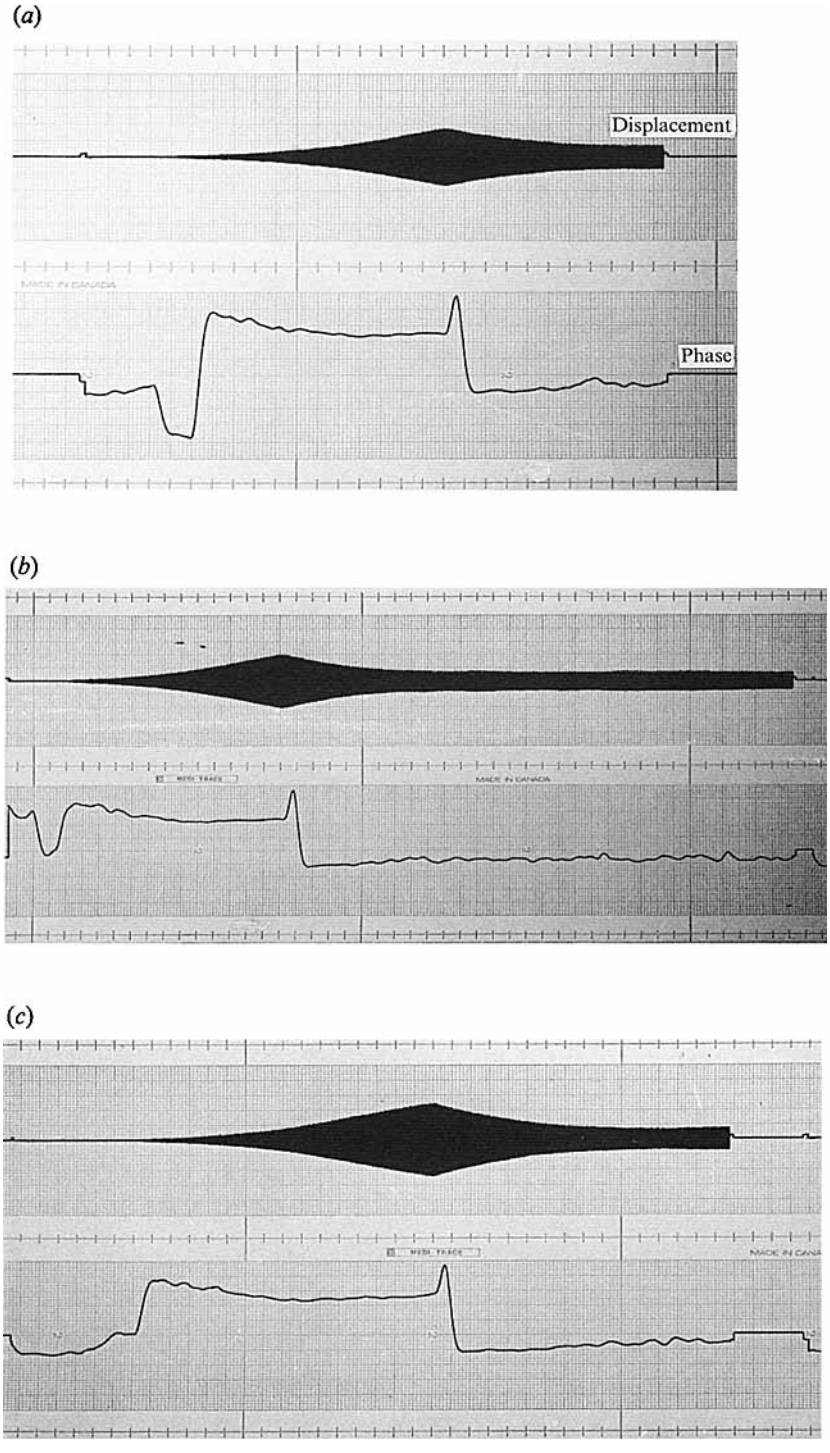

FIGURE 10. Breaks at different levels of the vibration amplitude build-up from rest and the associated phase change Φ ($U = 0.87$). Upper trace, cylinder displacement; lower trace, phase angle Φ.

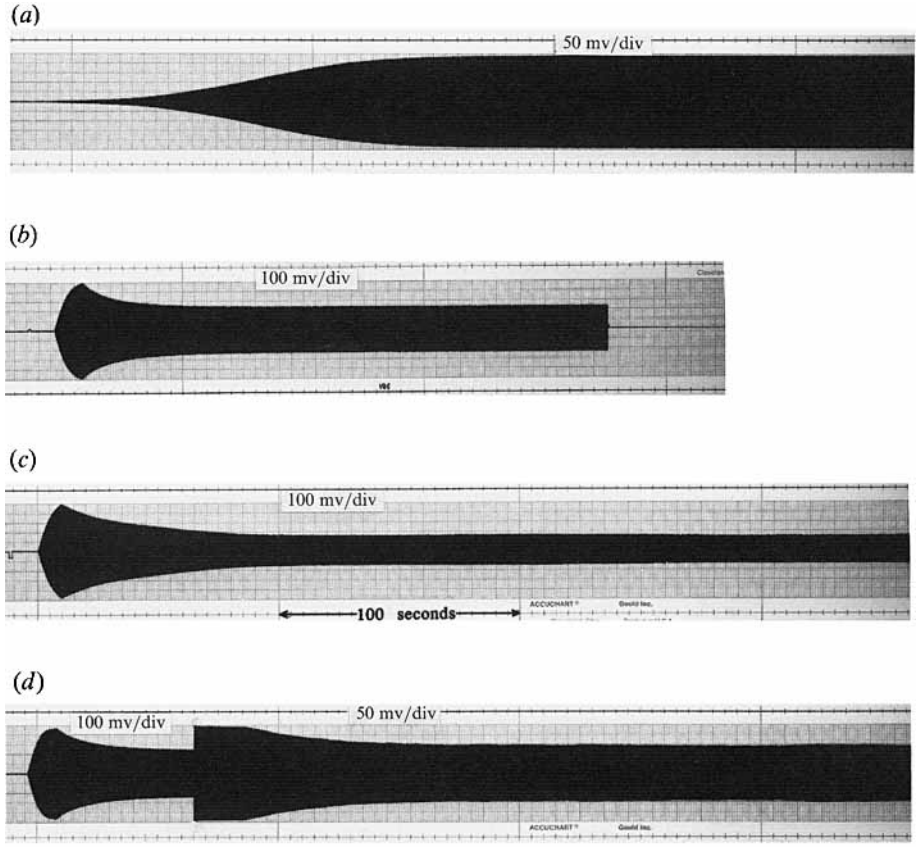

FIGURE 11. Records showing the two possible steady-state amplitudes for the velocity $U = 0.92$ obtained under different conditions: (*a*) from rest; (*b*), (*c*) and (*d*) with pre-excitation.

the case of the cylinder externally excited and released. Figures 11 (*a*) and 11 (*b*) indicate the same steady-state amplitudes for the two different procedures while the comparison of figure 11 (*b*) with 11 (*c*) shows that the final steady-state amplitude is not unique for the same procedure. Finally figure 11 (*d*) shows another intriguing behaviour (observed uniquely at this velocity): while the system appears to have settled at a first stationary amplitude which is identical to part (*b*), a break in the envelope curve occurs and the system converges towards the second stationary amplitude which happens to be identical to part (*c*). Note that the velocity is constant for all the results reported in figure 11.

3.2.3. *Build-up time to stationary oscillations*

For the impulsive regimes, it is observed that the time or the number of cycles required for the aeroelastic system to achieve steady-state oscillations depends of course on the initial amplitude and air velocity U, but also follows two different trends. Figure 12 shows for each steady amplitude A/D (circle symbols), the build-up time (triangle symbols) for the cylinder released from rest. For this lightly damped system, the build-up time increases exponentially with U during lock-in. In the range $0.78 \leqslant U \leqslant \text{LCV}$, the steady-state amplitudes are reached within two minutes while in the range $0.88 \leqslant U \leqslant 1.2$, the flow regime of the lower branch requires a significantly

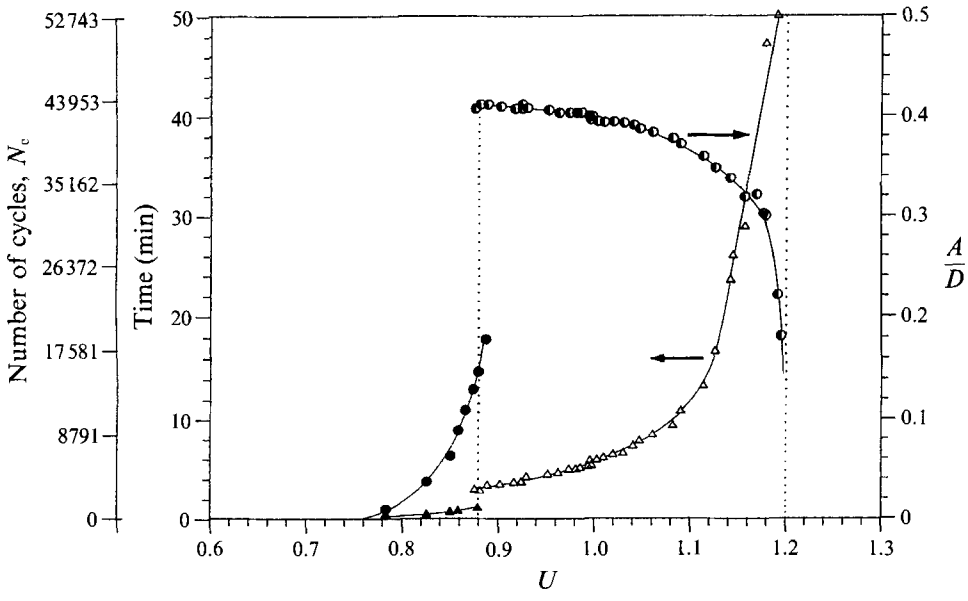

FIGURE 12. Build-up time from rest to steady-state oscillations: △, ▲, build-up time; ◐, ●, amplitude.

longer time to be established, double at the common point $U = 0.88$, and over 50 minutes at $U = 1.2$.

Figure 13 shows the data for the cylinder externally pumped to about $A/D = 0.85$ and then released. Compared to the previous figure, it can be observed again that in the range $0.88 \leqslant U \leqslant 0.96$, two stationary amplitudes of oscillations can exist and that their rate of decay is much less important than in the case of the cylinder released from rest.

If two boundaries are defined, the first at the end of synchronization ($U = 1.2$, in this case) and the second at the jump of the lower branch (LCV), the resulting domain I can be associated with the flow regime of the lower branch, the 2P vortex mode, following the notation of Williamson & Roshko (1988). The domain II defined by $0.78 \leqslant U \leqslant$ LCV can be associated with the flow regime of the upper branch (2S vortex mode). It is interesting to observe that the flow regime 2P is limited to domain I while the 2S regime, present in domain II, also invades domain I up to $U = 0.96$. According to figure 13, when the 2S regime takes precedence over the 2P regime, its decay time is longer than in the 2P case while, according to figure 12 the build-up time for the 2P regime is always longer than that for the 2S regime.

3.3. *Spanwise variation of* Φ

Unlike experiments using a rigid cylinder, the present set-up allows for a spanwise variation of the cylinder amplitude. In order to investigate the spanwise coherence of the timing between the cylinder motion and the vortex shedding, the phase Φ is measured at several axial positions. As shown in figure 14, the ratio of the local phase to the midspan value, Φ_x/Φ, is practically unity. In fact the phase remains constant within $\pm 5°$. This suggests that the flow mode is not influenced in this case by the vibration amplitude and consequently that results obtained with a rigid cylinder should compare well with the present ones. The flow mode can also be expected to be more influenced by a variation of the flow velocity.

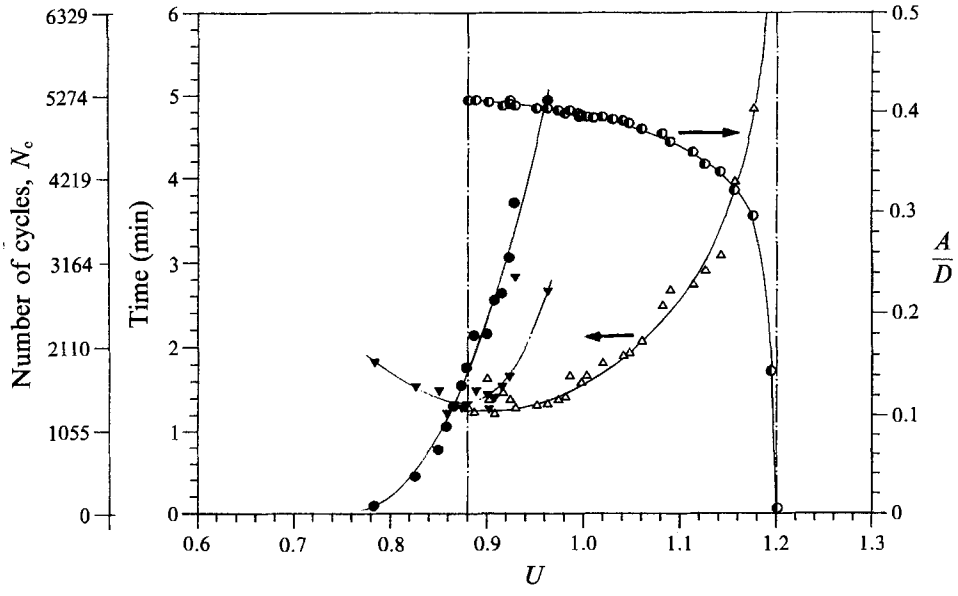

FIGURE 13. Decay time from a pre-excited amplitude to steady-state oscillations: △, ▼, decay time; ◐, ●, amplitude.

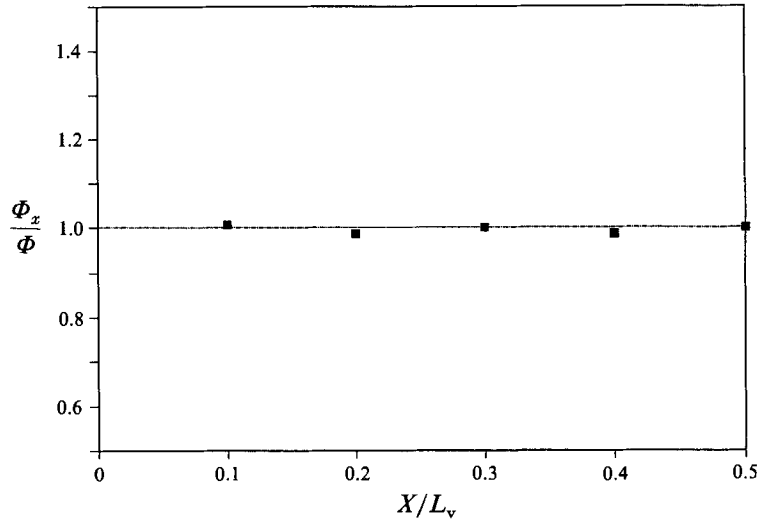

FIGURE 14. The spanwise variation of the phase angle ratio Φ_z/Φ ($U = 1.02$).

3.4. *Flow visualization of the cylinder near wake*

Figure 15 shows photographs of the vortex patterns in the cylinder near wake at $U = 0.93$ a velocity for which two steady-state amplitudes are possible. In both photographs, the flow is stroboscopically 'frozen' at the lower position of the cylinder vibration cycle.

The upper photograph (*a*) is obtained as the cylinder vibrates at a steady amplitude located on the upper branch of the hysteresis loop. The flow mode is clearly a 2S mode and the vortex is shed from the upper cylinder surface. The lower photograph (*b*) shows

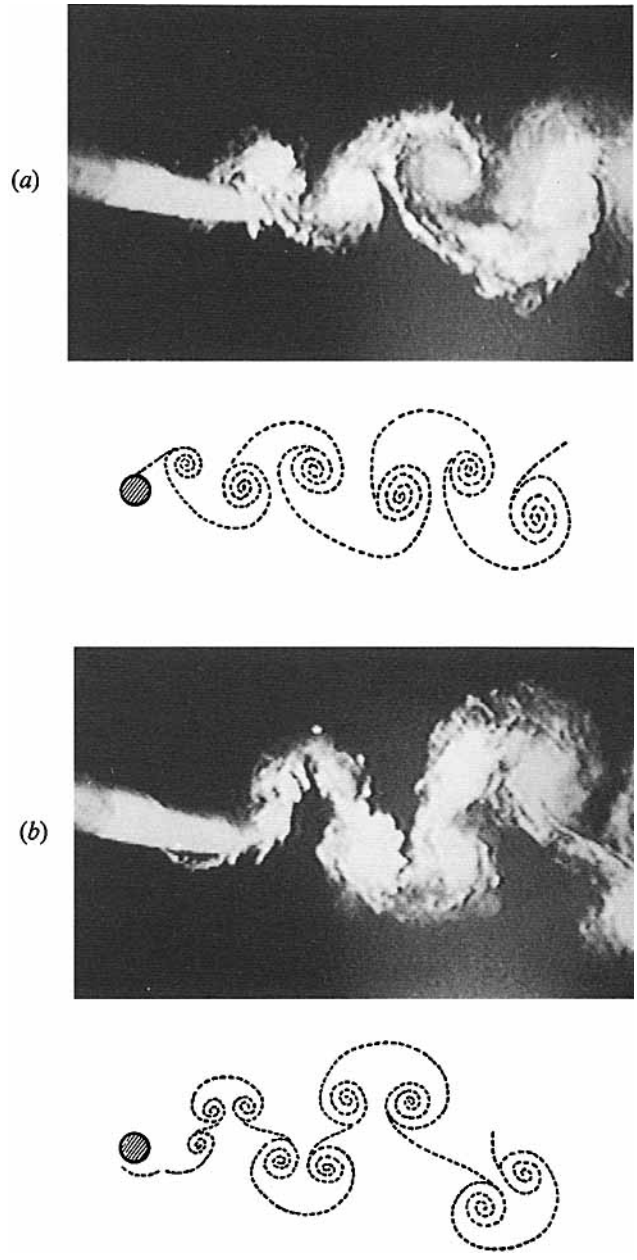

FIGURE 15. Photographs and sketches showing the two near-wake vortex patterns responsible for the hysteresis loop ($U = 0.93$, $Re = 7350$). (*a*) 2S mode ($A/D = 0.27$); (*b*) 2P mode ($A/D = 0.40$). Both photographs are taken at maximum negative displacement of the cylinder.

the near-wake flow as the cylinder oscillates at a steady amplitude but on the lower branch of the hysteresis loop. In this case the 2P mode is apparent and the vortex is now shed from the lower side of the model.

By comparing the two photographs, it appears that for the 2P mode, the vortices expand more laterally than for the 2S mode while convecting downstream. This behaviour agrees with the description given by Williamson & Roshko (1988).

Additional flow visualizations show that the jump from the upper branch to the lower one is accompanied by an instantaneous change from the 2S mode to the 2P mode.

In the case of bifurcation as the cylinder is released from rest (see figure 10), it was also observed that the initial flow mode, i.e. the 2P mode, converts suddenly to a 2S mode as the break in the amplitude envelope occurs.

From these flow visualization results, it can be concluded that the upper branch of the hysteresis loop is associated with the 2S mode, and the lower branch with the 2P mode.

4. Comparison and interpretation of the data

There are two approaches to the simulation of flow-induced vibrations: in the first, following Meier-Windhorst (1939), the oscillations of the cylinder mounted on an elastic system are allowed to develop freely with the flow and in the second, following den Hartog (1934), the oscillations are forced by an external system. The present study follows the Meier-Windhorst (1939) approach as did Feng in his simulation. Bishop & Hassan (1964*b*) adopted the den Hartog (1934) approach, as did Williamson & Rhosko (1988), Öngören & Rockwell (1988*a*, *b*) and Stansby (1976).

4.1. *Comparison with Feng's results*

In Feng's experiments, a rigid length of a circular model was mounted in a wind tunnel on an external air-bearing support system with adjustable linear springs and damping system. The cylinder displacement and the surface pressures were recorded. Each surface pressure tap was connected to a length of polyethylene tubing that was brought out through the end of the cylinder and connected to a pressure transducer mounted outside the wind tunnel. A calibration was done to account for the attenuation and phase lag of the pressure signal during transmission through the tubing.

Figure 16(*a*, *b*) shows a comparison of the dimensionless amplitudes of vibration as a function of the velocity U. Although the damping value ζ differs by one order of magnitude in the two experiments, the Scruton numbers are similar. The maximum A/D of the progressive regimes is almost identical (0.53) in both sets of data, as well as the upper branch of the hysteresis loop. The flow mode 2S associated with this upper branch does not appear influenced by the differences between these two experiments, i.e. the end conditions at the wall, the value of ζ (or the Scruton number) and the mode shape. The onset velocity associated with this upper branch occurs at $0.78 \leqslant U \leqslant 0.80$, and the upper branch hysteresis jump at $1.01 < U < 1.02$.

For the lower branch of the hysteresis loop, there is only one point of agreement, that is the end of the vortex-induced vibrations at $U \approx 1.28$. The amplitudes (A/D), the velocity U at which the jump occurs (0.89 in this experiment and 0.94 in Feng's experiment) and the synchronization plateau ($0.88 \leqslant U \leqslant 1.18$ in this experiment and $0.97 \leqslant U \leqslant 1.12$ in Feng's) all differ significantly. Clearly the flow mode 2P associated with the lower curve of the hysteresis loop is influenced by the experimental set-up.

For the impulsive regimes, both sets of data indicate that the upper branch of the hysteresis loop is not accessible for $U > 0.96$, but again, since this regime is related to the 2P flow mode, the data differ as in the progressive regimes.

The data of figure 17(*a*, *b*) show a comparison of the phase angle between the flow characteristic (surface pressure or hot-wire transducers) and the cylinder displacement signals. In both sets, the jumps in the A/D hysteresis loop are always accompanied by a sharp variation in Φ. Feng's data show a variation of 35° (by extrapolation) as the

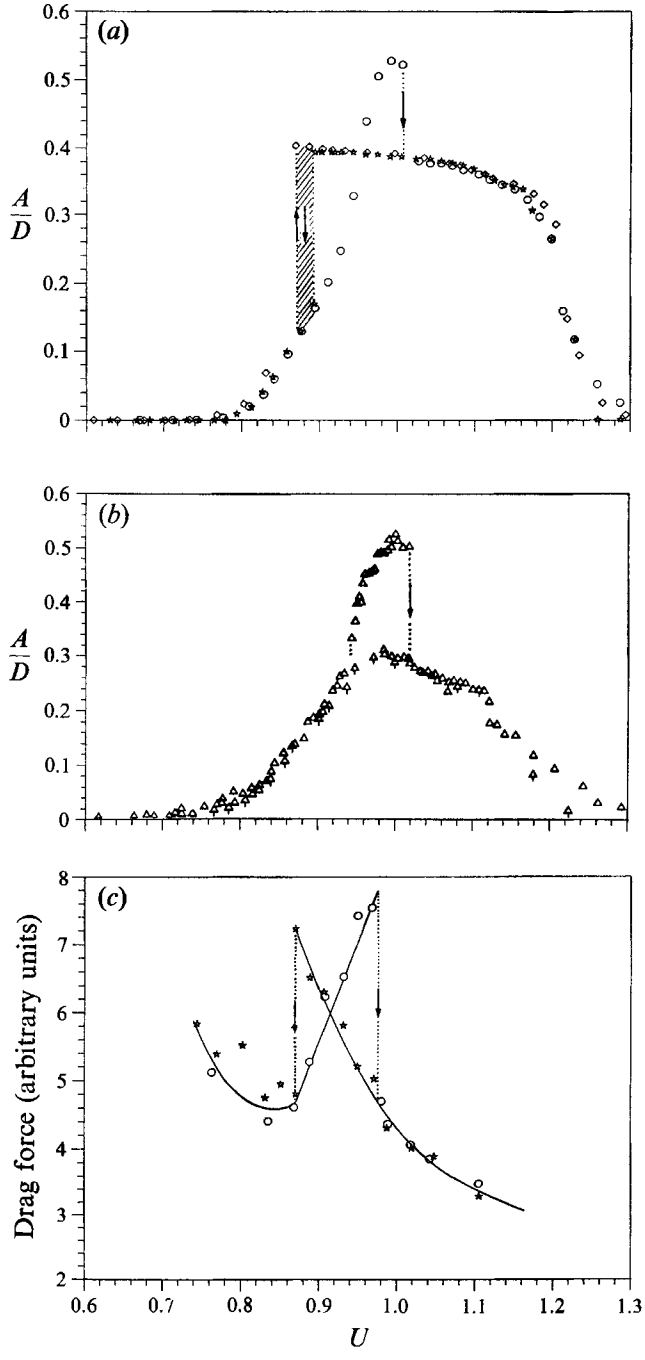

FIGURE 16. Comparison of the present results with those of Feng (1968) and Bishop & Hassan (1964*b*): (*a*) present study (symbols as in figure 6); (*b*) Feng's results: △, progressive regime; ▲, from rest; (*c*) Bishop & Hassan's results (drag force *vs.* U): ○, increasing velocity; ☆, decreasing velocity ($f_s = 2.923$ Hz; $A/D = 0.403$).

flow mode switches from 2S to 2P and of about 60° for the 2P → 2S jump. In the present data on the progressive regimes the phase angle varies by $\approx 75°$ as the flow mode changes from 2S to 2P at $U = 1.01$ and by $\approx 195°$ as the flow mode reverses from 2P to 2S at $U = 0.89$. In the cases of progressive regimes with large U increments and impulsive regimes, the jump from 2S to 2P mode can occur with a 190° variation in the phase angle ($U = 0.87$). It should be noted that the present data were averaged over 30000 to 60000 cycles.

Data for the ratio of the vortex shedding frequency to the cylinder natural frequency are compared in figure 18. Synchronization is obvious and the ratio f_{vs}/f_n is slightly lower in Feng's experiment than in the present one. As shown in the inset expanded graph, this ratio increases during lock-in in the progressive regimes (except for large U increments, open lozenge symbols) as U increases, but this increase remains very small, from 0.997 to 0.999. Outside the lock-in region, the vortex shedding frequency coincides with f_s.

4.2. *Comparison with Bishop & Hassan's results*

In their experiment, Bishop & Hassan (1964*b*) used the approach of forced vibrations. As their driving frequency was varied, which is equivalent to a variation of U, they found sudden changes in the lift and drag forces, accompanied by abrupt jumps in the phase angle between the forces and the cylinder displacement. Their system response was hysteretic since the critical frequencies (or U velocities) of these jumps depended on the vibration amplitude and the history of the motion (i.e. on whether the value of U was increased or decreased).

Some of their data are presented in figures 16(*c*) and 17(*c*) for comparison. The conversion from their variable f to the present variable U is achieved with the identity $U = (2\pi Sf/f_s)^{-1}$ using their measured f_s and a Strouhal number of 0.2 according to figure 9 of Bishop & Hassan (1964*a*).

Figure 16(*c*) shows the drag force variation for decreasing and increasing excitation frequencies while the oscillation amplitude was maintained at $A/D = 0.403$ which is the amplitude of the present free oscillations at the LCV. From this figure, the LCV is 0.87, matching that of the present study. However, the UCV have different values because of the difference in the oscillation amplitude ($A/D = 0.53$ for the present study).

Figure 17(*c*) shows the phase angle variation with U for two different amplitudes $A/D = 0.75$ (circle symbols) and $A/D = 0.20$ (triangle symbols). The variations are similar to those of the present study. The UCV is accompanied by an abrupt change of the phase angle by about 90°, while the LCV is accompanied by a more important change, of the order of 180° (by an extrapolation of the observed linear plateau). It can be noticed from this figure that the values of the phase Φ are influenced by the oscillation amplitude. They increase with increasing amplitude. The present phase angle results, once corrected for the hot-wire location, agree qualitatively and quantitatively with the ones of Bishop & Hassan (1964*b*).

4.3. *Comparison with flow visualization studies*

Two important papers report similar flow visualization studies designed to reveal the details of the flow in the near wake of an oscillating rigid circular cylinder in the synchronization region. In both studies – Öngören & Rockwell (1988*a*, *b*) and Williamson & Roshko (1988) – the rigid cylinder was forced to oscillate at given amplitudes and frequencies while exposed to a fixed relative waterflow velocity U. Öngören & Rockwell (1988*a*) observed in detail the change in the timing of the vortex

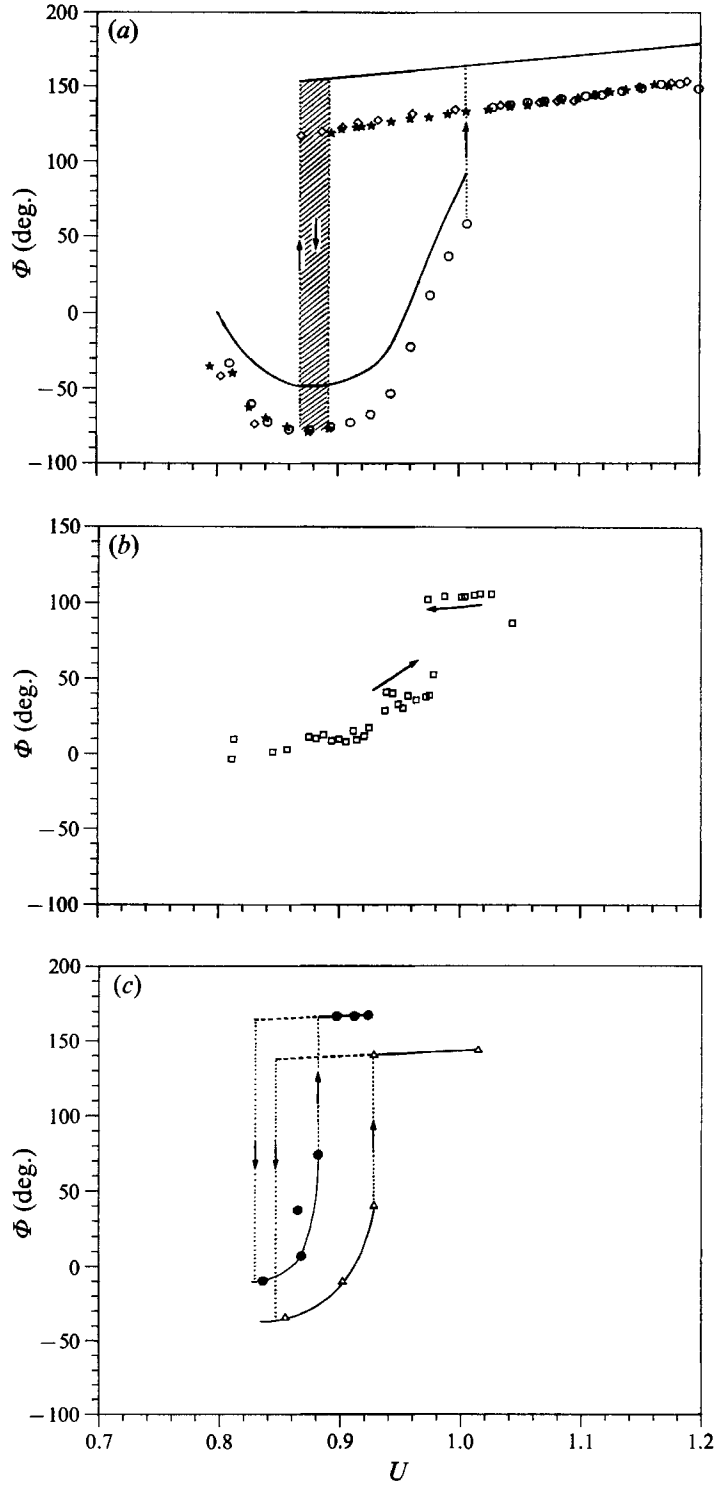

FIGURE 17. Comparison of the phase angle Φ results: (*a*) present study (symbols as in figure 6); ——, after correction; (*b*) Feng (1968); (*c*) Bishop & Hassan (1964*b*); ●, $A/D = 0.75$; △, $A/D = 0.20$; – – – –, extrapolated data.

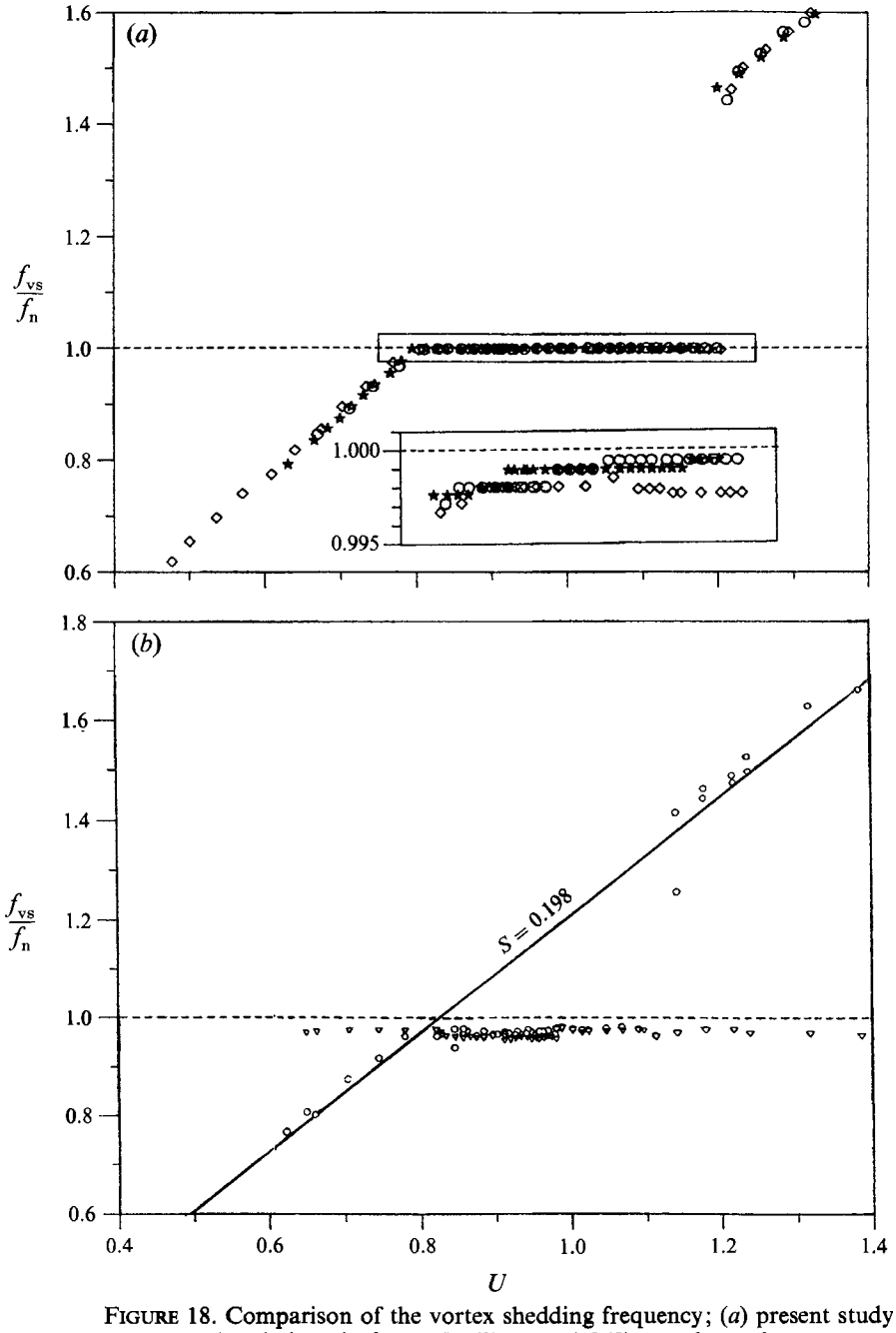

FIGURE 18. Comparison of the vortex shedding frequency; (*a*) present study (symbols as in figure 6); (*b*) Feng (1968): ▽, f; ○; f_{vs}.

shedding on either side of the phase jump. Williamson & Roshko (1988), in their interpretation of their flow visualization results also provide an explanation for the hysteresis loop in terms of a change in the configuration of the vortex wake. Figure 19, adapted from their paper, gives the boundaries of the relevant vortex configurations, denoted by codes 2S and 2P as mentioned earlier. Figure 19 does not include the regions within which superharmonic or subharmonic vortex shedding modes have been

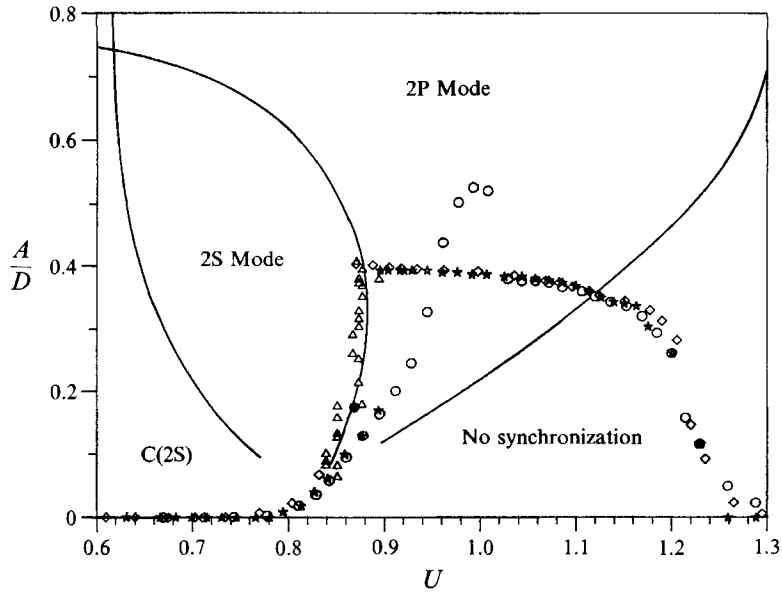

FIGURE 19. Present results compared with those of Williamson & Roshko (1988): ○, increasing velocity; ☆, decreasing velocity; ◇, increasing velocity with large steps; △, bifurcation amplitude; ●, bifurcation amplitude (Ferguson 1965); ——, Williamson & Roshko (1988).

found (Öngören & Rockwell 1988*a*) and deals with the zones containing patterns near the fundamental synchronization region. In the present free vortex-induced vibrations, the oscillation frequency is practically the flexible cylinder natural frequency and the abscissa is translated in terms of U with the relation $\lambda/D = 2\pi U$, where λ is the cylinder vibration wavelength (V/f).

The present results, superimposed in the figure, support most of the flow visualization results. The agreement on the definition of the 'critical curve', the boundary between 2S and 2P modes, is remarkable.

The plateau of the hysteresis lower branch obtained in the progressive regime with decrements of U, begins at $U = 1.14$, close to the boundary between the 2P mode and the zone where no synchronized pattern is observed and terminates at $U = 0.87$ or the LCV, which is a point on the critical curve.

As observed for the impulsive regimes, in the range $0.78 \leqslant U \leqslant$ LCV, the vibration build-up from rest, at a fixed U can be disturbed and cease to converge towards a first stationary amplitude for a second stationary amplitude. In this velocity range, the initial vortex mode at small vibration amplitudes of the cylinder appears to be of the 2P type. As the amplitude builds up, the boundary between 2P–2S modes, the critical curve, is reached and the 2S mode takes over, a manifestation accompanied by an abrupt change in the phase angle. For a velocity U in the same range but close to the LCV (see figure 10), the amplitudes of these bifurcations were recorded and their location (triangle symbols of figure 19) confirmed the critical curve. Ferguson (1965) made a similar observation of an instantaneous break in the cylinder amplitude for $U = 0.87$. His experimental result can be seen to coincide with the boundary between the 2S–2P modes (see the filled circle of figure 19). Around $U =$ LCV, the 'critical curve' is almost vertical and this explains the susceptibility to a 2P → 2S mode jump at several amplitudes.

In the range $0.84 \leqslant U \leqslant 0.87$, say 0.86, for an impulsive regime the cylinder with an

initial $A/D = 0.85$ excitation amplitude could undergo, according to figure 19, two phase angle changes, the first while moving from the 2P to the 2S mode at $A/D = 0.45$ and the second at $A/D = 0.18$ switching back to the 2P mode. This phenomenon of a double mode jump has not been observed. Once the cylinder amplitude falls into the 2S mode, natural Kármán vortex shedding prevails. This prevalence of the 2S mode is also observed for progressive regimes with small increments. At the onset of synchronization, the vortex pattern of the stationary vibrations corresponds to a 2S mode and is preserved in the 2P mode region, following the upper curve of the hysteresis loop as the air velocity is slowly increased. There is competition between the 2P and 2S modes up to $U = 1.01$, where the 2P mode takes over as shown by a 75° change in the phase angle (35° in Feng's results). The coexistence of different modes was also observed by Öngören & Rockwell (1988*b*) but for a cylinder vibrating at a non-orthogonal angle with the flow. This coexistence takes the form of a first mode controlling the far wake and a second one, the near wake. As the air velocity U is increased, the first mode progresses upstream and finally dislodges the second mode.

The longer build-up times required for the 2P mode to establish the stationary amplitudes, as observed in the present data (§3.2.2), is an indication that the 2P mode is the weaker of the two, a weakness associated with the lateral expansion of its wake and to the pairing of smaller and opposite signed vortices.

Comparing the wake flow patterns observed by Griffin & Ramberg (1974), Öngören & Rockwell (1988*a*) and Williamson & Roshko (1988) with the present photographs shown in figure 15, it is interesting to note that the Reynolds number of the present tests ($Re = 7350$) introduces turbulent characteristics superimposed over the more regular patterns obtained at lower Reynolds numbers. Nevertheless, the 2S and 2P modes can be clearly recognized and the earlier explanation suggested by Williamson & Roshko for the hysteresis loop in terms of a change in the wake vortex patterns is confirmed.

5. Conclusions

An experimental investigation of the free vortex-induced vibrations of a long flexible circular cylinder with a low damping ratio shows that the cylinder steady response is hysteretic as the flow velocity is varied, and that the hysteresis is a fluid-mechanic phenomenon.

The hysteresis loop is characterized by two branches and, as shown by flow visualization, each branch is associated with a particular vortex shedding mode and delimited by a discontinuity featuring a jump to the other branch. The upper branch obtained by small progressive increments of the flow velocity and extending from the onset of synchronization ($U = 0.78$) to the upper critical velocity ($U = 1.01$) is associated with the von Kármán type wake or the 2S mode of vortex shedding suggested by Williamson & Roshko (1988). The lower branch of the hysteresis is obtained either by progressive decrements of the flow velocity or by releasing the cylinder from rest under a fixed flow velocity. The lower branch covers a velocity range extending from a lower critical velocity ($U = 0.88$) to the end of synchronization ($U = 1.2$) and is associated with the 2P mode in which two vortices of opposite sign are shed from each side of the cylinder at every vibration cycle (Williamson & Roshko). The 2P mode is also the final regime for the range $0.96 < U < 1.2$ if the cylinder is pumped to a high amplitude and then released. Over a narrow range ($0.88 < U < 0.96$) and for this particular impulsive regime, the cylinder is observed to stabilize on either one of

the two branches. The probability of the existence of the 2S mode decreases as U increases.

The results of the present study agree partially with those obtained by Feng (1968). With different damping ratios but almost identical Scruton numbers, the maximum steady vibration amplitude is of the same order, while the synchronization covers a larger velocity range, and the hysteresis loop covers a velocity range twice as large. In the study by Bishop & Hassan (1964*b*) and the present one, a jump in the phase angle of the order of π occurs at the same lower critical velocity and another jump of the order of $\frac{1}{2}\pi$ at the upper critical velocity.

For fluid velocities less than the lower critical velocity, where a 2P → 2S mode jump appears, the cylinder oscillation amplitude grows as it is released from rest towards a first stationary amplitude and then bifurcates towards a second stationary amplitude. The amplitudes of the bifurcation occurrence coincide with the critical curve separating the 2S mode and 2P mode regions defined by Williamson & Roshko. The bifurcation is accompanied by a sudden change of the phase angle between the fluid excitation and the cylinder displacement. A flow visualization confirms that the initial 2P mode of vortex shedding jumps to a 2S mode as this bifurcation takes place.

The authors would like to thank Dr D. Noiseux for helpful discussions and are pleased to acknowledge the financial support of Hydro-Quebec, the Natural Science and Engineering Research Council of Canada and the Education and Scientific Research Ministry of Algeria.

REFERENCES

ANGRILLI, F., DI SILVIO, G. & ZANARDO, D. 1974 Hydroelasticity study of a circular cylinder in a water stream. In *Flow-induced Structural Vibrations* (ed. E. Naudascher), pp. 504–512. Springer.

BATCHELOR, G. K. 1967 *An Introduction to Fluid Dynamics*. Cambridge University Press.

BEARMAN, P. W. 1984 Vortex shedding from oscillating bluff bodies. *Ann. Rev. Fluid Mech.* **16**, 195–222.

BERGER, E. 1984 Zwei Fundamentale Aspekte Wirbelerregter Schwingungen. *German-Fottinger, Institut Für Thermo-und Fluiddynamik, Berlin*, 343/12.

BISHOP, R. E. D. & HASSAN, A. Y. 1964*a* The lift and drag forces on a circular cylinder in a flowing fluid. *Proc. R. Soc. Lond.* A **277**, 32–50.

BISHOP, R. E. D. & HASSAN, A. Y. 1964*b* The lift and drag forces on a circular cylinder oscillating in a flowing fluid. *Proc. R. Soc. Lond.* A **277**, 51–75.

BLEVINS, R. D. 1977 *Flow-Induced Vibration*. Van Nostrand Reinhold.

BRIKA, D. 1990 Étude expérimentale des vibrations éoliennes d'un cylindre flexible à différentes incidences. PhD thesis, Université de Sherbrooke.

CHEN, Y. N. 1972 Fluctuating lift forces of Kármán vortex street on single circular cylinder and in tube bundles. Part 1: the vortex street geometry of the single circular cylinder. *Trans. ASME* **B**: *J. Engng Indust.* **94**, 603–612.

FENG, C. C. 1968 The measurement of vortex-induced effects in flow past stationary and oscillating circular and D-Section cylinders. MASc thesis, University of British Columbia.

FERGUSON, N. 1965 The measurement of wake and surface effects in the subcritical flow past a circular cylinder at rest and in vortex-excited oscillation. MASc thesis, University of British Columbia.

GRIFFIN, O. M. & RAMBERG, S. E. 1974 The vortex street wakes of vibrating cylinders. *J. Fluid Mech.* **66**, 553–576.

HARTLEN, R. T. & CURRIE, J. G. 1970 Lift oscillator model of vortex induced vibration. *J. Engng Mech. Div. ASCE* **96** (EM5), 577–591.

HARTOG, J. P. DEN 1934 The vibration problem in engineering. *Proc. 4th Intl Cong. Appl. Mech., Cambridge*, pp. 36–53.

HOLMES, P. J. & RAND, D. A. 1976 The bifurcation of Duffing's equation: an application of catastrophe theory. *J. Sound Vib.* **44**, 237–253.

LANDL, R. 1975 A mathematical model for vortex-excited vibrations of bluff bodies. *J. Sound Vib.* **42**, 219–234.

MEIER-WINDHORST, A. 1939 Flatterschwingungen von zylindern in gleichmässigen Flüssigkeitsstrom. *Mitteilungen Hydraul. Inst. Techn. Hochschule, München*, **9**, 3–9.

ÖNGÖREN, A. & ROCKWELL, D. 1988*a* Flow structure from an oscillating cylinder. Part 1. Mechanisms of phase shift and recovery in the near wake. *J. Fluid Mech.* **191**, 197–223.

ÖNGÖREN, A. & ROCKWELL, D. 1988*b* Flow structure from an oscillating cylinder. Part 2. Mode competition in the near wake. *J. Fluid Mech.* **191**, 225–245.

PANKHURST, R. C. & HOLDER, D. W. 1962 *Wind Tunnel Technique*. Pitman.

PARKINSON, G. V. 1989 Phenomena and modelling of flow-induced vibrations of bluff bodies. *Prog. Aerospace Sci.* **26**, 169–224.

RAWLINS, C. B. 1983 Wind tunnel measurements of the power imported to a model of a vibrating conductor. *IEEE Trans. Pow. App. Syst.* PAS **102**, 963–971.

SARPKAYA, T. 1979 Vortex-induced oscillations – A selective review. *Trans. ASME* E: *J. Appl. Mech.* **46**, 241–258.

STANSBY, P. K. 1976 Base pressure of oscillating circular cylinders. *J. Engng Mech. Div. ASCE* **102** (EM4), 591–600.

WILLIAMSON, C. H. K. & ROSHKO, A. 1988 Vortex formation in the wake of an oscillating cylinder. *J. Fluids Struct.* **2**, 355–381.

ZDRAVKOVICH, M. M. 1982 Modification of vortex shedding in the synchronization range. *Trans. ASME* I: *J. Fluids Engng* **104**, 513–517.